Performance of Magnetic Quantum Cellular Automata and Limitations Due to Thermal Noise

Federico M. Spedalieri, Ajey P. Jacob, *Member, IEEE*, Dmitri E. Nikonov, *Senior Member, IEEE*, and Vwani P. Roychowdhury

***Abstract*—Operation parameters of magnetic quantum cellular automata are evaluated for the purposes of reliable logic operation. The dynamics of the nanomagnets is simulated via the Landau–Lifshitz–Gilbert equations with a stochastic magnetic field corresponding to thermal fluctuations. It is found that in the macrospin approximation, the switching speed does not change under scaling of both size and distances between nanomagnets. Thermal fluctuations put a limitation on the size of nanomagnets: when we consider a majority gate that features a biaxial anisotropy as a stabilizing mechanism and a uniform clocking field, the gate error rate becomes excessive for nanomagnets smaller than about 200 nm at room temperature.**

***Index Terms*—Bit error rate, magnetic logic devices, majority gate, micromagnetic simulation, nanomagnets, thermal fluctuations.**

I. Introduction

THE SUCCESS of computing in the past 40 years was based on scaling the CMOS transistors to the nanoscale size [1]. As it is anticipated that this scaling will approach limits defined by the quantum theory and thermodynamics [2], the search is on for alternative logic technologies [3], [4], which would be able to supplement CMOS and have certain advantages compared to it. One promising technology among them is spintronics and nanomagnetics [5].

Magnetic quantum cellular automata (MQCA) have been proposed as one of the types of spintronic logic. MQCA are based on bistable nanomagnet elements that can perform basic logic operations by means of magnetostatic interactions. Nanomagnets are typically arranged in the shape of crosses—majority gates. A majority gate has three inputs and one output. The output's logic state is determined by the "majority voting" of the logic states of the inputs. This gate is naturally suited for the magnetic dipole–dipole interaction that is the basis of MQCA. It also allows us to perform AND and OR logical functions by fixing one of the inputs, and (in combination with the NOT element) it can be used to perform any logical operation. Another type of spintronics—domain-wall logic [6] can also be rendered in the form of majority gates [7]. A chain of nanomagnets carrying the logic variables was demonstrated by Cowburn and Welland [8]. Later, a majority gate based on these principles was proposed and experimentally implemented [9].

To be a viable alternative to CMOS logic, MQCA must show that they can achieve a better (or at least similar) performance level at least in one of the benchmarks, such as size, speed, switching energy, bit stability, and scalability. Some of these issues have been studied through simulations [10], [11]. In this paper, our goal is to estimate how far can we push the limits of MQCA performance for all the aforementioned benchmarks. To this end, we will analyze a simplified model of MQCA that captures the basic physical principles that govern its behavior. We pay a special attention to the limitation stemming from the thermal fluctuations of the magnetization.

The paper is organized as follows. In Section II, we show how the bit stability of an MQCA element puts a lower bound on its size. In Section III, we introduce a simple model of the MQCA dynamics and use it to simulate the behavior of an MQCA majority gate and study the speed of a signal propagating along a chain of nanomagnets. In Section IV, we discuss the relationship between MQCA initialization and its stability. In Section V, we simulate the effects of thermal fluctuations and study their impact on the error rate of the majority gate. Finally, in Section VI, we summarize our results and present our conclusions.

II. Bit Stability and Minimum Size

Our first step will be to study what type of constraints bit stability imposes on the size of MQCA. The basic element of MQCA is a nanomagnet that is used to store a single bit of information. Usually the nanomagnets are elongated along some direction, which determines the easy axis of magnetization due to shape anisotropy. This bit is represented by the magnetization direction of this nanomagnet: "0" for the magnetization "pointing up," i.e., along positive easy axis, and "1" for the magnetization "pointing down," i.e., along negative easy axis. We thus need to require these two configurations to be stable and separated by an energy barrier to prevent bit-flip errors. Even though material properties such as the uniaxial anisotropy can be exploited to produce such a bistable system, shape anisotropy is more advantageous to produce such a result because it provides an easier way to control the energy barrier by lithographic patterning, and most proposals of MQCA are essentially based on this idea.

Manuscript received August 6, 2009; revised January 12, 2010; accepted April 24, 2010. Date of publication May 27, 2010; date of current version May 11, 2011. The work of F. M. Spedalieri and V. P. Roychowdhury was supported by the Nanoelectronics Research Initiative from the Western Institute of Nanoelectronics, and by the Microelectronics Advanced Research Corporation, through the Focus Center for Materials, Structures and Devices. The review of this paper was arranged by Associate Editor D. Litvinov.

F. M. Spedalieri and V. P. Roychowdhury are with the Department of Electrical Engineering, University of California, Los Angeles, CA 90095 USA (e-mail: federico@ee.ucla.edu; vwani@ee.ucla.edu).

A. P. Jacob and D. E. Nikonov are with the Components Research, Technology and Manufacturing Group, Intel Corporation, Santa Clara, CA 95052 USA (e-mail: ajey.p.jacob@intel.com; dmitri.e.nikonov@intel.com).

Digital Object Identifier 10.1109/TNANO.2010.2050597

Our mathematical model is based on the free energy of a nanomagnet with uniform magnetization $\mathbf{M}$. It includes contributions from the shape anisotropy, material anisotropy, and the energy in the external magnetic field (see [12] for a derivation)

$$E = K_1(1-(\mathbf{m}\cdot\hat{\mathbf{e}}_{\text{axis}})^2)V + \frac{1}{2}\mu_0 M_s^2 V \mathbf{m}\cdot\mathcal{N}\cdot\mathbf{m} - \mu_0 M_s V \mathbf{m}\cdot\mathbf{H}_{\text{ext}} \quad (1)$$

where $\mathbf{m} = \mathbf{M}/M_s$ is the normalized magnetization (note that $|\mathbf{m}| = 1$), M_s is the saturation magnetization of the material, V is the volume of the nanomagnet, μ_0 is the permeability of vacuum, K_1 is the uniaxial anisotropy of the material, $\hat{\mathbf{e}}_{\text{axis}}$ is a unit vector in the direction of the easy axis, $\mathcal{N}$ is the demagnetizing tensor, and $\mathbf{H}_{\text{ext}}$ is the external field. The demagnetizing tensor can be diagonalized by finding its principal axis, and its diagonal elements are positive and satisfy $N_x + N_y + N_z = 1$. We will consider that our nanomagnet is a rectangular prism whose symmetry axes are aligned with the cartesian axes. We will also assume that the easy axis of the crystalline uniaxial anisotropy is aligned with the y-axis. The explicit expression for these demagnetizing factors can be found in [13].

Let us consider the case of a vanishing external field. If a, b, and c are the dimensions of the nanomagnet in the x, y, and z directions, respectively, we will assume that $b > a > c$, which corresponds to a rectangular prism elongated in the y-direction. This choice of proportions translates into an inverse ordering of the demagnetizing factors ($N_z > N_x > N_y$). This makes the z-direction the least energetically favorable. It is easy to see that the energy is minimal when the magnetization points in the y-direction, either up or down. These are the two stable states that encode a bit of information. Then, the energy barrier between these two minima is smaller when we consider the magnetization to be in the x–y plane. To compute this energy barrier, we just need to evaluate (1) in the x- and y-directions and subtract them. Then, we have

$$\Delta E = E(\mathbf{m} = \hat{\mathbf{e}}_x) - E(\mathbf{m} = \hat{\mathbf{e}}_y) = \frac{1}{2}\mu_0 M_s^2 V\left[N_x - \left(N_y - \frac{2K_1}{\mu_0 M_s^2}\right)\right]. \quad (2)$$

From this equation, we can extract a few useful facts: 1) the energy scale is given by $(1/2)\mu_0 M_s^2 V$; 2) the energy barrier, and hence, the energy dissipation, scales down with the volume of the nanomagnet; 3) the geometrical anisotropy can be used to control the height of the barrier; and 4) the uniaxial crystal anisotropy can be seen as a correction to the geometrical anisotropy.

The height of the energy barrier will determine the stability of the information stored in the nanomagnets, and hence, its bit stability. The thermal fluctuations will cause the direction of the magnetization to vary and with a certain probability to turn over 90°—the direction of the energy saddle point. After that, the magnetization will flip to the other energy minimum. In a simple model, the probability of the nanomagnet's magnetization flips its direction due to thermal noise is given by $p_{\text{flip}} = \exp(-\Delta E/k_B T)$, where k_B is the Boltzmann constant. Since we are interested in MQCA as an alternative to CMOS-based logic, it is natural to require this error probability to be at least of the same order as that of CMOS transistors, which is of the order of 10^{-17}. This corresponds to the condition $\Delta E/k_B T > 40$. For room temperature, we have $k_B T \approx 0.026$ eV, and so we need $\Delta E \approx 1$ eV or larger. The energy barrier height gives an approximate estimate of the energy that will be dissipated every time we switch the magnetization direction of a nanomagnet. The exception would be slow adiabatic switching regime, which according to [14] applies for clocking field ramp-up times of around 7 ns and longer. In this paper, we will only consider instantaneous variations of the clocking field, well outside the adiabatic regime.

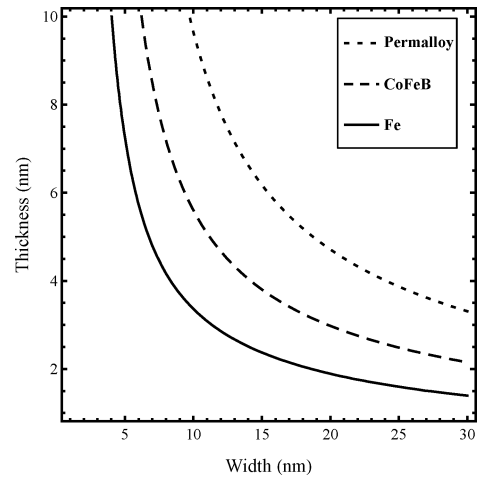

Fig. 1. Thickness versus width for a nanomagnet with an energy barrier of 1 eV. The length is taken to be twice the width.

The lower bound on the height of the energy barrier, coupled with (2) allows us to extract a lower bound on the size of the nanomagnets. Since the energy barrier depends on the volume of the nanomagnet, any lower bound on it will translate into a lower bound on the volume. Assuming that the geometrical anisotropy is due to a 2:1 aspect ratio between the length and width of the prism, we can plot the values of thickness and width that are required to obtain a 1 eV energy barrier. In Fig. 1, we present this plot for three different materials: permalloy, CoFeB, and Fe (with saturation magnetizations equal to 800, 1180, and 1750 kA/m, respectively). For example, in permalloy, we can see that for a thickness of 6 nm, the nanomagnet needs to have a 15 nm width and a 30 nm length. Clearly, there is an advantage for higher values of the saturation magnetization, since we can achieve the same energy barrier height with a smaller volume (2).

It can be argued that the very high bit stability we are requiring (error rate $\simeq 10^{-17}$) might be appropriate for a memory device, but may not need to be that high for a logic device. For MQCA, we only need the nanomagnets to maintain their state only during the time it takes to perform a certain computation. We might be able to reduce the size even further, if we somewhat relax the bit stability requirements. However, given that the dependence of the error probability with the energy barrier is exponential, a small reduction in size can have a huge impact on the bit stability. We can illustrate this point by repeating the plot in Fig. 1 for

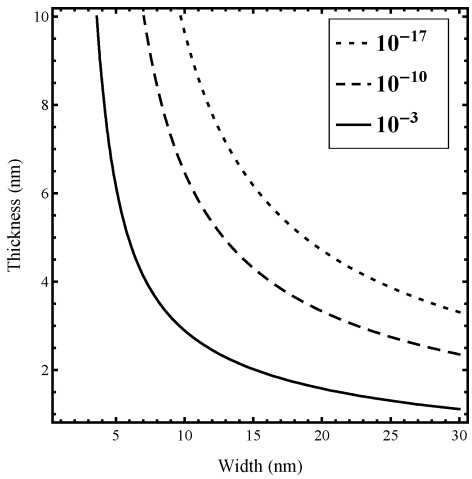

Fig. 2. Thickness versus width for different values of the error probability (plot corresponds to permalloy and a 2:1 aspect ratio).

permalloy, but for different values of the error probability (see Fig. 2). We can see the rapid increase of the error probability even for a modest reduction on the size of the nanomagnet. This shows that the lower limit on the size of MQCA is a rather strong one, if we want to preserve bit stability.

III. Dynamics and Speed

To estimate the speed of MQCA-based logic devices, we will simulate their behavior using the Landau–Lifshitz–Gilbert (LLG) equations [15], [16]. Since we are only interested in an order of magnitude estimate, we will skip the detailed micromagnetic simulations that are usually discussed in the literature [17], and instead work with a very simple model of the MQCA. We will model each nanomagnet as a macrospin, but we will include the effects of geometrical and crystalline anisotropies in the computation of the effective field. This approximation is equivalent to assuming the magnetization is uniform over the whole volume of a nanomagnet at any time, and neglecting magnetic moments higher than the dipole moment [11], [18]. We expect this approximation for improvement in decreasing nanomagnet size, since the exchange interaction tends to force the magnetization to be uniform on a length scale of about 10 nm. From our discussion in earlier section, we are interested in nanomagnet sizes of the order of tens of nanometers; therefore, we are not that far from that regime. In any case, we are interested in an upper bound for the speed of MQCA-based logic, and a full simulation will most likely produce a slower device.

The LLG equations [19], [20] for the macrospin model are

$$\frac{d\mathbf{M}^{(i)}}{dt} = -\frac{\gamma}{1+\alpha^2}\mathbf{M}^{(i)} \times \mathbf{H}_{\text{eff}}^{(i)} - \frac{\gamma\alpha}{(1+\alpha^2)M_s}\mathbf{M}^{(i)} \times (\mathbf{M}^{(i)} \times \mathbf{H}_{\text{eff}}^{(i)}) \quad (3)$$

where $\mathbf{M}^{(i)}$ is the magnetization of the ith nanomagnet, $\mathbf{H}_{\text{eff}}^{(i)}$ is the effective field at the position of the ith nanomagnet, $\gamma = g|e|/2m_e c = 2.21 \times 10^5\ \text{mA}^{-1} \cdot \text{sec}^{-1}$ is the Lande factor, and α is the Gilbert damping constant, which depends on the material and the environment of the nanomagnet and typically has values in the range 0.001–0.1. The effective field includes the contributions of any external field, the nanomagnet self-field, and the field due to the dipole–dipole interaction with other nanomagnets

$$\mathbf{H}_{\text{eff}}^{(i)} = \mathbf{H}_{\text{ext}}^{(i)} - \mathcal{N} \cdot \mathbf{M}^{(i)} + \sum_j \mathbf{C}_{(ij)}\mathbf{M}^{(j)}. \quad (4)$$

In this expression, we are assuming that all nanomagnets have the same shape, and hence, the demagnetizing tensor $\mathcal{N}$ is the same for all nanomagnets. This term can also include the effects of uniaxial crystalline anisotropy, if we redefine the corresponding demagnetizing factor $N_y \to N_y - (2K_1)/\mu_0 M_s^2$, where y is the easy axis of the crystalline anisotropy. The last term on the right-hand side (RHS) of (4) represents the dipole–dipole interaction between nanomagnets, and the matrices $\mathbf{C}_{(ij)}$ are coupling constants determined by their size and relative positions. If $(x^{(i)}, y^{(i)}, z^{(i)})$ are the coordinates of the ith nanomagnet, we define the coordinate differences for a pair of nanomagnets as $d_x^{(ij)} = x^{(i)} - x^{(j)}$, $d_y^{(ij)} = y^{(i)} - y^{(j)}$, $d_z^{(ij)} = z^{(i)} - z^{(j)}$, and the distance between nanomagnet centers as $d^{(ij)} = \sqrt{(d_x^{(ij)})^2 + (d_y^{(ij)})^2 + (d_x^{(ij)})^2}$. If we define a vector $\mathbf{d}^{(ij)} = (d_x^{(ij)}, d_y^{(ij)}, d_z^{(ij)})$, we can write the coupling constant matrices $\mathbf{C}_{(ij)}$ as

$$\mathbf{C}_{(ij)} = \frac{V^{(j)}}{4\pi(d^{(ij)})^5}\left(3(\mathbf{d}^{(ij)})^{\mathbf{T}} \cdot \mathbf{d}^{(ij)} - d^{(ij)}\mathbf{I}\right) \quad (5)$$

where $\mathbf{I}$ is the identity matrix. In our case, since all nanomagnets will be in the (x, y) plane, this expression simplifies, since $d_z^{(ij)} = 0$. An important fact about the matrices $\mathbf{C}_{(ij)}$ is that they are dimensionless, and hence, invariant under scaling of both the sizes of nanomagnets and the distances between nanomagnets. We will see that this property is preserved by the LLG equations in our model.

To simplify the simulation and analysis, it is useful to normalize the LLG equations. This is accomplished using the following definitions:

$$\mathbf{m}^{(i)} = \frac{\mathbf{M}^{(i)}}{M_s}$$
$$\mathbf{h}_{\text{eff}}^{(i)} = \frac{\mathbf{H}_{\text{eff}}^{(i)}}{M_s}$$
$$t' = t(\gamma M_s) \quad (6)$$

where now all the quantities on the left-hand side (LHS) of (6) are dimensionless (note that $[\gamma M_s] = \text{s}^{-1}$). With these rescalings and using vector identities and the obvious fact that $d\mathbf{M}^{(i)}/dt.\mathbf{M}^{(i)} = 0$, we can rewrite the normalized LLG equations in an implicit form that simplifies the implementation of the simulation

$$\frac{d\mathbf{m}^{(i)}}{dt'} = -\mathbf{m}^{(i)} \times \mathbf{h}_{\text{eff}}^{(i)} + \alpha\mathbf{m}^{(i)} \times \frac{d\mathbf{m}^{(i)}}{dt'}. \quad (7)$$

These equations have the property that the value of the magnetization is constant $|\mathbf{m}^{(i)}(t')| \equiv 1\,\forall t'$ and this feature must be preserved in the discretized numerical model. To do this, we

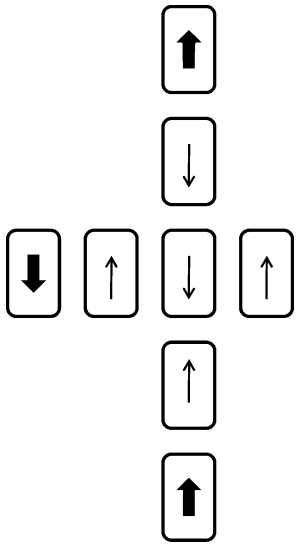

Fig. 3. Majority gate: the thick arrows represent nanomagnets with fixed magnetization that simulate inputs to the gate. The remaining nanomagnet align their magnetization in order to minimize the energy of the system from an initial magnetization in the x-(horizontal) direction. The output of the gates can be extracted from the magnetization of the "output" nanomagnet on the right.

employ the midpoint method [21] with which this constraint is automatically satisfied.

To estimate the speed with which MQCA switch, we simulated the behavior of the majority gate. Let us first briefly review its operation. The nanomagnets forming the gate are arranged as seen in Fig. 3. We also include three nanomagnets with fixed magnetization that are used to simulate the inputs of the gate. The nanomagnets that form the gate are initially magnetized in the x-direction, and then are left to evolve driven by the magnetic dipole interaction. The magnetization of each nanomagnet will tend to align itself with the field produced by the other nanomagnets at its position. The geometric anisotropy will force the magnetization to lay in the y-direction, and the influence of other nanomagnets will decide if it ends pointing up or down. The fields of the three inputs will add at the position of the central magnet and decide its direction of magnetization, hence computing the majority of the input signals. Finally, this signal can be read on the output magnet. Note that a signal that propagates horizontally is inverted every time it is received by the next nanomagnet (due to the antiferromagnetic coupling). This does not affect the function of the gate, although this feature must be tracked in order to correctly interpret the output of any MQCA-based gate.

Again, in order to extract numerical estimates from the simulation, we specified the properties of the material (M_s and K_1) to be those of permalloy. The value of the Gilbert damping constant did not have a big effect on the simulation when confined to the typical range 0.001–0.01. We found that the typical gate time, measured as the time it took the output to reach 90% of its final magnetization, was about 700 ps. An interesting feature of our model is that the normalized equations (7) are invariant under changes of scale, which means that *the gate time is independent of size*. Even though this is only true in this simplified model, and making less approximations will likely break this invariance, whatever effects this may have on the the gate time will likely be of higher order. This is in contrast to CMOS logic [1] as well as MQCA based on magnetic wires (rather than discrete nanomagnets) [7].

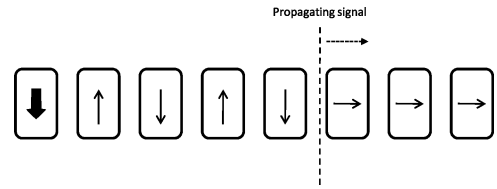

Fig. 4. Signal propagation through a horizontal wire made up of a chain of nanomagnets. The antiferromagnetic coupling forces neighboring nanomagnets to become antiparallel.

From the form of the normalized equations, we can see that the speed of this gate will depend on the material properties. In particular, the speed of the gate increases linearly with the saturation magnetization of the material. This follows from the scaling of actual time t with respect to normalized time t', as defined by (6).

Another issue that needs to be considered, when analyzing the speed of MQCA-based information processing, is the speed of propagation of information. In MQCA, this is accomplished by chains of nanomagnets that are initially magnetized in the x-direction, and evolve according to the dipole–dipole interaction propagating a signal, as can be seen in Fig. 4 for the case of a horizontal wire. Note that the antiferromagnetic coupling forces neighboring nanomagnets are antiparallel. For vertical wires, the coupling is ferromagnetic and the nanomagnets magnetization tends to become parallel.

This evolution follows the same dynamical equations presented in the earlier section; therefore, we can use them to simulate the propagation of a signal along a chain of nanomagnets and estimate its speed. For nanomagnets made of permalloy with a width of about 10 nm, separated by 15 nm, the speed of signal propagation is around 100 m/s, or equivalently, 150 ps per magnet. This is of the order of the speed of sound, and would certainly limit the speed of an integrated MQCA chip, if communication is done using the same principles as logic. This speed depends on the material through the saturation magnetization, but only linearly; therefore, it is not likely that choosing a different material will solve this problem for MQCA.

IV. Initialization and Bit Stability

As discussed earlier, in order to run a MQCA-based logic gate, it is necessary to initialize the magnetization of all nanomagnets in the x-direction (i.e., the hard axis.) In terms of energy, this corresponds to placing all nanomagnets at the top of the energy barrier created by the geometrical and crystalline anisotropies [see Fig. 5(a)]. However, this configuration corresponds to an unstable equilibrium point for each nanomagnet, and it should be expected that small perturbations due to thermal effects and stray fields will randomly force the nanomagnets to relax to one of their stable configurations independent from the input signals.

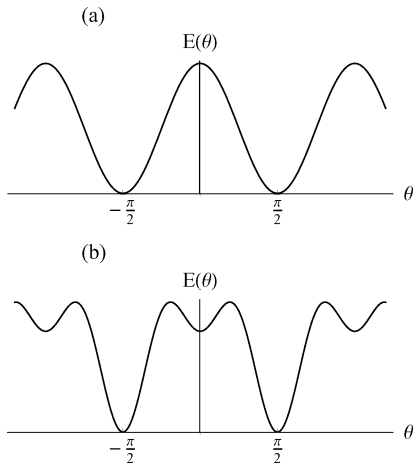

Fig. 5. (a) Energy profile for geometrical and uniaxial anisotropies. Stable configurations correspond to magnetization in the y-direction (up or down). Magnetization in the x-direction (initial configuration) is an unstable equilibrium point. (b) Including a biaxial anisotropy produces local minima for magnetization in the x-direction, stabilizing the initial configuration.

This is an important issue for any implementation of MQCA-based logic, and some possible solutions have been suggested. One consists of exploiting the biaxial anisotropy of the material to create a stable configuration around the initialization direction, by generating a local minimum of the energy [22]. If we consider the magnetization confined to the x–y plane, and note θ as the angle between the magnetization direction and the x-axis, the geometric and uniaxial anisotropy result in an energy profile proportional to $\cos^2(\theta)$, as can be seen in Fig. 5(a). The biaxial anisotropy introduces another term that is proportional to $\sin^2(2\theta)$, and by carefully choosing the parameters, we can produce a local minimum for $\theta = 0$, as seen in Fig. 5(b).

This energy minimum provides a latch mechanism that keeps the initialized nanomagnets pointing in the x-direction while the information from the input signal propagates through the chain of magnets. Once again, the effectiveness of this local minimum to trap the magnetization direction against thermal fluctuations will depend on the height of the energy barrier around it [i.e., the energy difference between the peaks and the local minimum in Fig. 5(b)]. The reasoning of Section II applies to estimate the energy of this barrier necessary to preserve the bit in its local energy minimum for sufficiently long time, and hence, obtain an estimate of the strength of the required biaxial anisotropy. We realize that the requirements to the height of this barrier are contradictory—it should be high enough to prevent spontaneous transition to one of the global minima before the signal reaches the bit; it also needs to be low enough so that the signal can reliably switch it to the desired local minimum. In the following section, we simulate the behavior of the majority gate, including the biaxial anisotropy, in the presence of thermal fluctuations.

V. Thermal Effects and Gate Error Probability

In this section, we model the effects of the thermal fluctuations on the operation of MQCA. We especially focus on gate errors caused by spontaneous transitions from the local energy minimum after the initialization of elements of MQCA.

Our simulations will use the stochastic LLG equations based on the midpoint rule derived by d'Aquino *et al.* in [21]. The only difference with the aforementioned model (see Section III) will be the inclusion of an extra term that represents the field generated by the biaxial anisotropy (we show in the appendix that the introduction of this term does not affect the useful properties of the discretized equations.)

Let us start by considering the extra term in the normalized effective field that is responsible for the biaxial anisotropy acting on nanomagnet (i)

$$\begin{aligned}\mathbf{h}^{(i)}_{\mathrm{eff\,(biaxial)}} = -\frac{2K_2}{\mu_0 M_s^2}\big(&m_x^{(i)}(1-(m_x^{(i)})^2)\hat{\mathbf{x}} \\ &+ m_y^{(i)}(1-(m_y^{(i)})^2)\hat{\mathbf{y}} \\ &+ m_z^{(i)}(1-(m_z^{(i)})^2)\hat{\mathbf{z}}\big). \end{aligned} \tag{8}$$

The biaxial anisotropy constant K_2 has dimensions of $\mathrm{J}\cdot\mathrm{m}^{-3}$. It is not difficult to show that, when restricted to the x–y plane, the contribution to the energy of this term is proportional to $\sin^2(2\theta)$, where θ is the angle between the magnetization direction and the x-axis. In order to have a local minimum around $\theta = 0$, the constant K_2 must satisfy the condition

$$K_2 > K_{2\min} = \frac{1}{2}\mu_0 M_s^2 V\left[N_x - \left(N_y - \frac{2K_1}{\mu_0 M_s^2}\right)\right]. \tag{9}$$

The thermal fluctuations manifest themselves as random variations of the overall magnetization of the nanomagnet. We describe this process by the stochastic LLG equations [23], [24], which are obtained by adding a random force, or, in other words, a stochastic thermal magnetic field $\mathbf{h}_T^{(i)}(t)$ to the effective field in (7). Note that we are considering a different thermal field for each nanomagnet, since it is usually assumed that the thermal fluctuations in different nanomagnets are uncorrelated. The random thermal field $\mathbf{h}_T^{(i)}(t)$ is assumed to be an isotropic vector Gaussian white-noise process with variance ν^2, and therefore, it can be expressed in terms of the Wiener process as $\mathbf{h}_T^{(i)}(t)dt = \nu\, d\mathbf{W}^{(i)}$. Then, the stochastic LLG equations take the form

$$\begin{aligned} d\mathbf{m}^{(i)} = &-\mathbf{m}^{(i)} \times \big(\mathbf{h}^{(i)}_{\mathrm{eff}} + \mathbf{h}^{(i)}_{\mathrm{eff\,(biaxial)}}\big)dt \\ &- \mathbf{m}^{(i)} \times \nu\, d\mathbf{W}^{(i)} + \alpha\, \mathbf{m}^{(i)} \times d\mathbf{m}^{(i)}. \end{aligned} \tag{10}$$

The value of ν can be obtained from the fluctuation dissipation theorem in thermal equilibrium, and is given by $\nu = \sqrt{2\alpha k_B T/\mu_0 M_s^2 V}$.

Using (10), we simulated the behavior of the majority gate for various values of size, damping constant, and temperature. We fixed the saturation magnetization and uniaxial anisotropy to be those of permalloy, and studied the error rate of the gate as a function of K_2 and for several values of the damping constant α. Starting with the nanomagnets initialized with magnetization in the x-direction, each run simulated the evolution of the gate for 2000 ps. We considered the gate to be successful, if the average of the output magnet during the last 300 ps was

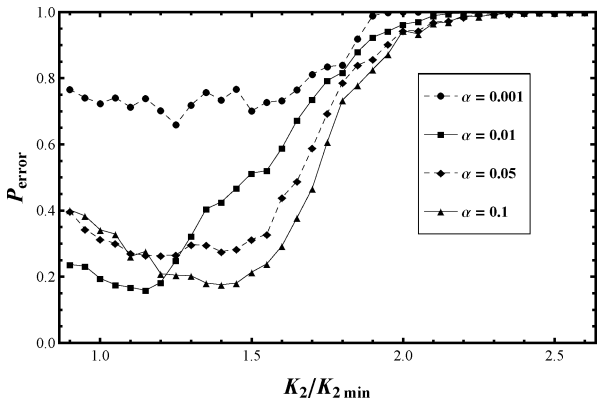

Fig. 6. Error probability of the majority gate as a function of the (scaled) biaxial anisotropy for different values of the damping constant ($T = 300$ K).

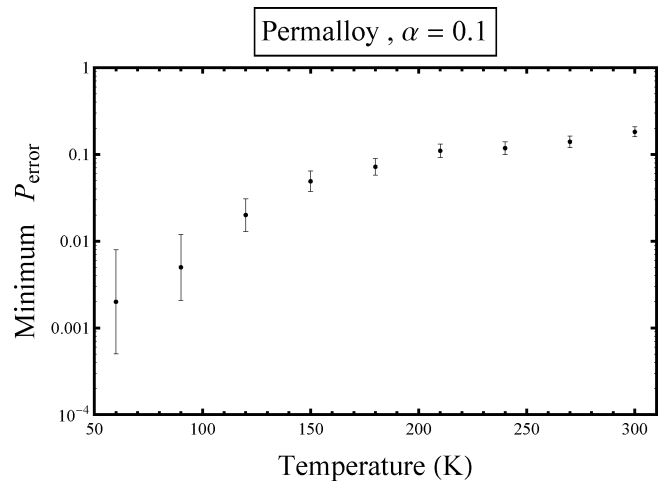

Fig. 7. Minimum error probability of the majority gate as a function of temperature.

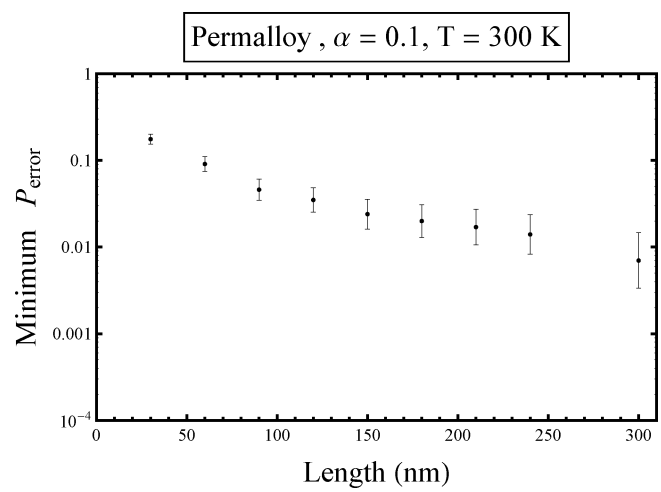

Fig. 8. Minimum error probability of the majority gate as a function of the length of the nanomagnets.

larger than 80% of the ideal output value (all runs used the same set of fixed inputs.) In any other case, we considered that the gate failed. For each value of the parameters K_2 and α, we ran 1000 instances of the simulation. The results are presented in Fig. 6. The error probability is plotted against the ratio of K_2 to $K_{2\min}$, where $K_{2\min}$ is the minimum value of the biaxial anisotropy that produces a local energy minimum around $\theta = 0$. If we increase K_2, we expect the error probability to decrease when we pass $K_2/K_{2\min} = 1$, since the biaxial anisotropy becomes more effective in preventing a premature flipping of the nanomagnets spurred by the thermal fluctuations. On the other hand, if we increase the biaxial anisotropy too much, the local energy minimum is too deep for the signal to force the nanomagnet to flip. This is the behavior we can appreciate in Fig. 6. For $K_2 > 2K_{2\min}$, the gate becomes essentially frozen by the biaxial anisotropy; for $K_{2\min} < K_2 < 2K_{2\min}$, the error probability seems to have a minimum for a certain value of K_2 that depends on the damping constant. However, an important result of these simulations is that for the particular temperature and size considered (30 nm $\times$ 15 nm $\times$ 6 nm magnets), the gate error rate exceeds a certain minimum value, 15% in this case. The stabilizing effects of the biaxial anisotropy are either too weak, and spontaneous gate errors happen, or too strong so that it prevents the normal evolution of the gate.

One possible solution for the gate error probability will be to decrease the temperature. Then, thermal fluctuations will be weaker and smaller values of the biaxial anisotropy will be enough to keep the magnets magnetized in the x-direction until the signal, in the form of the magnetization of a neighboring magnet in the y-direction, reaches the magnet and makes it flip up or down, and since the required biaxial anisotropy is not too large, it does not freeze the magnet in its initial magnetization direction. We used our model to study the dependence of the gate error probability on the temperature, again running 1000 simulations for each value of the temperature and the biaxial anisotropy, and then finding the minimum value of the error probability for each temperature. These results are presented in Fig. 7.

We can see that, as expected, the error probability decreases with decreasing temperature, although this decrease seems rather slow for temperatures above 150 K. For temperatures below 30 K, the error probability is below 0.001, but it could not be accurately estimated with the same number of simulation runs.

Another approach to lowering the error probability of the gate is to increase the size of the magnets. We know that larger magnets have a larger energy barrier between the states of up and down magnetization. This increases the stability of the computational states of the magnets, but it is not the reason why the majority gate becomes more reliable. The key parameter is the ratio of the height of the energy barrier surrounding the local energy minimum around the magnetization in the x-direction and the strength of the signal produced by neighboring magnets. We ran our simulations for different sizes of the nanomagnets, but keeping a 2:1 aspect ratio and a thickness of 6 nm. Figs. 8 and 9 show the results for $\alpha = 0.1$ and $\alpha = 0.01$, respectively.

For both values of α, we can see that the error probability decreases fast with size. The mechanism for this behavior is the following. When we increase the size of the magnets following

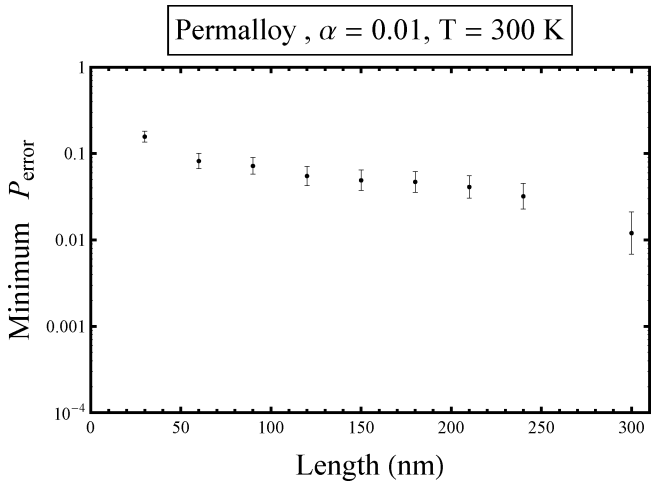

Fig. 9. Minimum error probability of the majority gate as a function of the length of the nanomagnets.

the aforementioned prescription, the depth of the local minimum increases, but this increase is approximately a linear function of the length. On the other hand, the volume of the magnet increases quadratically with the length (since we are keeping a fixed aspect ratio), and hence, the strength of the magnetic field generated by the magnets also increases quadratically. The deeper local minimum does a better job in stabilizing the magnet against thermal fluctuations, while the magnetic interaction grows faster, preventing the biaxial anisotropy from freezing the nanomagnets. By comparing the simulation results for the two values of the damping constant, we can see that damping plays a dual role. On the one hand, it corresponds to stronger magnetic noise and thus a larger tendency of the nanomagnet to escape from the quasi-stable equilibrium state. On the other hand, damping causes a force that drives the nanomagnet toward the quasi-stable equilibrium. As a result, simulations show that both for $\alpha = 0.1$ and $\alpha = 0.01$, the probability of error are of the same order of magnitude. From these results, we can also see that nanomagnets with size less than 200 nm have too high gate error probability and thus cannot be used to build MQCA.

VI. Conclusion

The goal of this study was to estimate the characteristics of an MQCA-based logic device, in particular, the limits that can be achieved in terms of minimum size, gate-switching time, switching energy, and gate error probability. To this end, we analyzed a simplified model in an effort to understand how these features are affected by the basic parameters that characterize the MQCA. A reasonable requirement on the bit stability of these devices naturally leads to a lower bound on the size of the basic element of any MQCA. A nanomagnet must be at least 20 nm long in one of its dimensions to prevent thermal fluctuations from inducing an error rate larger than that of today's CMOS transistors. Furthermore, reducing this size results in a rapidly degrading bit stability of the components, making its applications in logic circuits less useful. Fault-tolerant design does not seem to help in this situation, since any reduction in the size of the nanomagnets will be offset by the increase in their number due to the overhead usually accompanies fault-tolerant implementations. Another way to push beyond this limit would be to work at much lower temperatures, but that regime will not be practical in the most common situations.

The lower bound on size also provides us with an estimate of switching for MQCA. After initialization of an MQCA, energy is dissipated when the magnetization of each nanomagnet "rolls down" the energy barrier until it reaches a minimum energy configuration (like a ball rolling on curved surface in the presence of friction.) Then, the energy dissipated by each nanomagnet is just the energy it had at the top of the barrier, and that is just the height of the barrier. From the bit stability constraint, we found that this height should be at least 1 eV, and hence, a MQCA could, in principle, dissipate about 1 eV per nanomagnet. A logic gate such as the majority gate requires only five nanomagnets; therefore, we could perform logic functions with a switching energy as low as a few electronvolts. This is a big advantage of MQCA over CMOS transistors that requires several thousand electronvolts to operate [25]. This is, however, only a theoretical limit, and it does not take into account the practical difficulties of efficiently transferring such a small amount of energy to each nanomagnet.

To estimate the speed of MQCA logic gates, we considered a very simple model in which we approximated the nanomagnets by point dipoles when computing their interaction, but included the effects of geometrical and crystalline anisotropies through the computation of the effective field. This approach is less sophisticated than the micromagnetic simulations that have been used in the literature to study similar systems; our goal was not to obtain a very detailed picture of the dynamics, but rather to have a good estimate of the fastest gate time MQCA can achieve. Our model includes all the fundamental elements of MQCA dynamics, and more refined simulations are likely to result in slower gate times. Using this simple model, we found that the majority gate produces the required output in about 700 ps, which is slower than gate times expected from CMOS in the next few years.

Another obstacle for implementing MQCA-based logic has to do with information transmission. In MQCA, this is accomplished following the same basic principles as logic. Chains of nanomagnets propagate a signal through the dipole–dipole interaction. But the propagation speed of this signal turns out to be around 100 m/s, which is extremely slow when compared with the speed of electric signals in a wire (typically around 10^7 m/s.) This is a huge disadvantage for any MQCA scheme.

MQCA suffers from the problem that its nanomagnets are initialized in an unstable state before the computation. Thermal fluctuation will push the nanomagnets randomly into one of the stable states, regardless of the value prescribed by the computation. It has been proposed [22] that exploiting the biaxial anisotropy of the material can increase the robustness of the MQCA initial state against thermal fluctuations, preventing premature relaxation of the nanomagnets before the computation is complete. On the other hand, a strong biaxial anisotropy can completely freeze the dynamics, by trapping the magnetization in the local energy minimum of the initial state. We simulated

the behavior of the majority gate in the presence of thermal fluctuations and analyzed the error rate of the majority gate for different values of the biaxial anisotropy in order to find what are the optimal choices of the parameters. We found that for room temperature operation ($T = 300$ K), the gate error rate has an impractically high value ($> 1\%$) for all sizes of nanomagnet smaller than 200 nm. This seems to show that the biaxial anisotropy approach may not be enough to solve the gate error rate problem, and scale MQCA logic to smaller sizes at room temperature.

Appendix

Properties of the Discretized Stochastic LLG Equations

In this appendix, we show some of the details of the numerical approach used to solve the stochastic LLG equations in the presence of thermal fields. As mentioned earlier, we follow essentially the approach presented in [21] that uses the midpoint rule to discretize the stochastic LLG equations. Here, we will show that introducing an extra term in the effective field that represents the effects of the biaxial anisotropy does not change the two main properties of this technique, namely, the unconditional preservation of the magnetization magnitude and the consistency of the evolution of the free energy.

The stochastic LLG equations take the form

$$d\mathbf{m}^{(i)} = -\mathbf{m}^{(i)} \times \mathbf{h}_{\text{eff}}^{(i)} dt - \mathbf{m}^{(i)} \times \nu d\mathbf{W}^{(i)} + \alpha \mathbf{m}^{(i)} \times d\mathbf{m}^{(i)} \tag{11}$$

where $\mathbf{h}_{\text{eff}}^{(i)}$ includes the biaxial term. Applying the midpoint method corresponds to the following replacements:

$$d\mathbf{m}^{(i)} \to \left(\mathbf{m}_{n+1}^{(i)} - \mathbf{m}_n^{(i)}\right) \tag{12}$$

$$\mathbf{m}^{(i)} \to \left(\frac{\mathbf{m}_{n+1}^{(i)} + \mathbf{m}_n^{(i)}}{2}\right) \tag{13}$$

$$\mathbf{h}_{\text{eff}}^{(i)}(\mathbf{m}^{(i)}, t_n) \to \mathbf{h}_{\text{eff}}^{(i)}\left(\frac{\mathbf{m}_{n+1}^{(i)} + \mathbf{m}_n^{(i)}}{2}, t_{n+\frac{1}{2}}\right) \tag{14}$$

$$d\mathbf{W}^{(i)} \to \left(\mathbf{W}_{n+1}^{(i)} - \mathbf{W}_n^{(i)}\right) \tag{15}$$

where $t_{n+(1/2)} = t_n + \Delta t/2$. These substitutions result in the discretized stochastic LLG equations

$$\left(\mathbf{m}_{n+1}^{(i)} - \mathbf{m}_n^{(i)}\right) = -\left(\frac{\mathbf{m}_{n+1}^{(i)} + \mathbf{m}_n^{(i)}}{2}\right) \times \mathbf{V} \tag{16}$$

where

$$\mathbf{V} = \mathbf{h}_{\text{eff}}^{(i)}\left(\frac{\mathbf{m}_{n+1}^{(i)} + \mathbf{m}_n^{(i)}}{2}, t_{n+\frac{1}{2}}\right)\Delta t + \nu\left(\mathbf{W}_{n+1}^{(i)} - \mathbf{W}_n^{(i)}\right) - \alpha\left(\mathbf{m}_{n+1}^{(i)} - \mathbf{m}_n^{(i)}\right). \tag{17}$$

Due to the form of (16), it is clear that the RHS vanishes when scalar is multiplied by $(\mathbf{m}_{n+1}^{(i)} + \mathbf{m}_n^{(i)})$, while the LHS becomes $(|\mathbf{m}_{n+1}^{(i)}|^2 - |\mathbf{m}_n^{(i)}|^2)$, and therefore, we have

$$|\mathbf{m}_{n+1}^{(i)}|^2 = |\mathbf{m}_n^{(i)}|^2 \tag{18}$$

which means the midpoint method unconditionally preserves the magnitude of the magnetization. Note that the form of the term added to the effective field does not affect this property, since the corresponding term on the RHS is still of the form $(\mathbf{m}_{n+1}^{(i)} + \mathbf{m}_n^{(i)}) \times \mathbf{U}$.

Another property that the discretized stochastic LLG equations presented in [21] have is that the change in the discretized free energy is bounded by the work performed by the thermal fields on the magnetization for any finite value of the increment Δt. Their proof of this fact relies on the particular form of the effective field, namely, the free energy is an at most quadratic polynomial function of the magnetization. Even though when we add the biaxial anisotropy term the free energy has a term of degree 4, the result still holds as shown in the following. First, we write the free energy $g(\mathbf{m})$

$$\begin{aligned} g(\mathbf{m}) = {} & \frac{1}{2}\sum_i \mathbf{m}^{(i)} \cdot \mathcal{N} \cdot \mathbf{m}^{(i)} - \sum_i \mathbf{h}_{ext}^{(i)} \cdot \mathbf{m}^{(i)} \\ & - \frac{1}{2}\sum_i \sum_{j \neq i} \mathbf{m}^{(i)} \cdot C^{(ij)} \cdot \mathbf{m}^{(j)} \\ & - \frac{2K_2}{\mu_0 M_s^2}\left(m_x(1 - m_x^2)\hat{\mathbf{x}}\right. \\ & \left. + m_y(1 - m_y^2)\hat{\mathbf{y}} + m_z(1 - m_z^2)\hat{\mathbf{z}}\right) \end{aligned} \tag{19}$$

where $\mathcal{N}$ is the demagnetization tensor that includes a term corresponding to the uniaxial anisotropy, $C^{(ij)}$ is the matrix that encodes the dipole–dipole interaction between nanomagnets (and it is symmetric with respect to i and j). We want to compute $g_{n+1} - g_n$, where $g_n = g(\mathbf{m}_n)$. Clearly, this will give us an expression in powers of $\delta\mathbf{m}^{(i)} = (\mathbf{m}_{n+1}^{(i)} - \mathbf{m}_n^{(i)})$. We will keep terms up to order $(\delta\mathbf{m}^{(i)})^2$, since from the LLG equations, we can see that $\delta\mathbf{m}^{(i)}$ is proportional to $(\mathbf{W}_{n+1}^{(i)} - \mathbf{W}_n^{(i)})$, and $(\mathbf{W}_{n+1}^{(i)} - \mathbf{W}_n^{(i)})^2$ is of order Δt . With that in mind, after some algebra, we get

$$\begin{aligned} g_{n+1} - g_n \simeq {} & \sum_i \left(\mathbf{m}^{(i)} \cdot \mathcal{N} - \sum_{j \neq i} \mathbf{m}^{(j)} \cdot C^{(ij)} \cdot \mathbf{m}^{(j)} - \mathbf{h}_{ext}^{(i)}\right. \\ & \left. - \mathbf{h}_{\text{biaxial}}^{(i)}\right) \cdot \delta\mathbf{m}^{(i)} + \frac{1}{2}\sum_i \delta\mathbf{m}^{(i)} \cdot \mathcal{N} \cdot \delta\mathbf{m}^{(i)} \\ & - \frac{1}{2}\sum_i \sum_{j \neq i} \delta\mathbf{m}^{(i)} \cdot C^{(ij)} \cdot \mathbf{m}^{(j)} \\ & - \frac{K_2}{\mu_0 M_s^2}\sum_i \delta\mathbf{m}^{(i)} \cdot \mathcal{D} \cdot \delta\mathbf{m}^{(i)} \end{aligned} \tag{20}$$

where $\mathcal{D} = \mathbf{1} + 2\mathbf{m}_n^{(i)}\mathbf{m}_n^{(i)\mathbf{T}} - 3\,\text{diag}((m_x^{(i)})_n^2, \quad (m_y^{(i)})_n^2, (m_z^{(i)})_n^2)$. Note that the term multiplying $\delta\mathbf{m}^{(i)}$ in the first sum is exactly $-\mathbf{h}_{\text{eff}}^{(i)}(\mathbf{m}_n)$ (as it should be). Now we go back to the

discretized LLG equations that have the form

$$\mathbf{m}_{n+1}^{(i)} - \mathbf{m}_n^{(i)} = -\mathbf{m}_{n+\frac{1}{2}}^{(i)} \times \left(\mathbf{h}_{\text{eff}}^{(i)} \left(\mathbf{m}_{n+\frac{1}{2}}^{(i)}, t_n + \frac{\Delta t}{2} \right) \Delta t + \nu \left(\mathbf{W}_{n+1}^{(i)} - \mathbf{W}_n^{(i)} \right) + \alpha \left(\mathbf{m}_{n+1}^{(i)} - \mathbf{m}_n^{(i)} \right) \right) \tag{21}$$

where now $\mathbf{h}_{\text{eff}}^{(i)}$ also includes the biaxial term. This equation is of the form $\mathbf{m}_{n+1}^{(i)} - \mathbf{m}_n^{(i)} = -\mathbf{m}_{n+(1/2)}^{(i)} \times \mathbf{A}$, and therefore, if we scalar multiply both sides by $\mathbf{A}$, the RHS vanishes and we get

$$\alpha |\delta \mathbf{m}^{(i)}|^2 = \mathbf{h}_{\text{eff}}^{(i)} \left(\mathbf{m}_{n+\frac{1}{2}}^{(i)}, t_n + \frac{\Delta t}{2} \right) \cdot \delta \mathbf{m}^{(i)} \, \Delta t + \nu \left(\mathbf{W}_{n+1}^{(i)} - \mathbf{W}_n^{(i)} \right) \cdot \delta \mathbf{m}^{(i)}. \tag{22}$$

Now we write $\mathbf{h}_{\text{eff}}^{(i)}(\mathbf{m}_{n+(1/2)}^{(i)}, t_n + (\Delta t/2))$ in terms of $\mathbf{h}_{\text{eff}}^{(i)}(\mathbf{m}_n^{(i)})$ (we drop the time, since the field does not have an explicit time dependence). After some more algebra, we get

$$\mathbf{h}_{\text{eff}}^{(i)} \left(\mathbf{m}_{n+(1/2)}^{(i)} \right) \cdot \delta \mathbf{m}^{(i)} = \mathbf{h}_{\text{eff}}^{(i)} \left(\mathbf{m}_n^{(i)} \right) \cdot \delta \mathbf{m}^{(i)} + \sum_{j \neq i} \delta \mathbf{m}^{(j)} \cdot C^{(ij)} \cdot \delta \mathbf{m}^{(i)} - \delta \mathbf{m}^{(i)} \cdot \mathbf{M}^{(i)} \cdot \delta \mathbf{m}^{(i)} \tag{23}$$

where $\mathbf{M}^{(i)} = (K_2/\mu_0 M_s^2)(3M^{(i)} - \mathbf{I}) - (1/2)\mathcal{N}$, with $M^{(i)} = \text{diag}((m_x^{(i)})_n^2, (m_x^{(i)})_n^2, (m_x^{(i)})_n^2)$. Now, using this in the expression, we computed for $g_{n+1} - g_n$, and doing even more algebra, we arrive to

$$g_{n+1} - g_n = \frac{\nu}{\Delta t} \sum_i \left(\mathbf{W}_{n+1}^{(i)} - \mathbf{W}_n^{(i)} \right) \cdot \delta \mathbf{m}^{(i)} - \sum_i \delta \mathbf{m}^{(j)} \cdot \mathcal{M}^{(i)}(\mathbf{m}_n) \cdot \delta \mathbf{m}^{(i)} \tag{24}$$

where $\mathcal{M}^{(i)}(\mathbf{m}_n) = (\alpha/\Delta t \mathbf{I}) + (2K_2/\mu_0 M_s^2)\, \mathbf{m}_n^{(i)} \mathbf{m}_n^{(i)\,\mathbf{T}}$. Hence, $\mathcal{M}^{(i)}(\mathbf{m}_n)$ is positive semidefinite, and therefore, we have finally

$$g_{n+1} - g_n \leq \nu (\mathbf{m}_{n+1}^{(i)} - \mathbf{m}_n^{(i)}) \cdot \frac{\left(\mathbf{W}_{n+1}^{(i)} - \mathbf{W}_n^{(i)} \right)}{\Delta t} \tag{25}$$

which shows that the change in the discretized free energy is always less than the work done by the stochastic field during the time interval Δt.

REFERENCES

[1] Semiconductor Industry Association, International Technology Roadmap for Semiconductors. (2007). [Online]. Available: http://public.itrs.net/

[2] V. V. Zhirnov, R. K. Cavin, J. A. Hutchby, and G. I. Bourianoff, "Limits to binary logic switch scaling - a gedanken model," *Proc. IEEE*, vol. 91, no. 11, pp. 1934–1939, Nov. 2003.

[3] G. I. Bourianoff, P. A. Gargini, and D. E. Nikonov. (2007). Research directions in beyond cmos computing. *Solid-State Electron.* [Online]. *51(11–12)*, pp. 1426–1431. Available: http://www.sciencedirect.com/science/article/B6TY5-4R4DG47-8/2/9b1406bbd2ddd0b134ca8a8717d31dea

[4] J. Hutchby, R. Cavin, V. Zhirnov, J. Brewer, and G. Bourianoff, "Emerging nanoscale memory and logic devices: A critical assessment," *Computer*, vol. 41, no. 5, pp. 28–32, May 2008.

[5] I. Žutić, J. Fabian, and S. D. Sarma, "Spintronics: Fundamentals and applications," *Rev. Mod. Phys.*, vol. 76, pp. 323–410, 2004.

[6] D. A. Allwood, G. Xiong, C. C. Faulkner, D. Atkinson, D. Petit, and R. P. Cowburn. (2005). Magnetic domain-wall logic. *Science* [Online]. *309(5741)*, pp. 1688–1692. Available: http://www.sciencemag.org/cgi/content/abstract/309/5741/1688

[7] D. E. Nikonov, G. I. Bourianoff, and P. A. Gargini, "Simulation of highly idealized, atomic scale magnetic quantum cellular automata logic circuits," *J. Nanoelectron. Optoelectronics*, vol. 3, pp. 3–11, 2008.

[8] R. P. Cowburn and M. E. Welland. (2000). Room temperature magnetic quantum cellular automata. *Science* [Online]. *287(5457)*, pp. 1466–1468. Available: http://www.sciencemag.org/cgi/content/abstract/287/5457/1466

[9] A. Imre, G. Csaba, L. Ji, A. Orlov, G. H. Bernstein, and W. Porod. (2006). Majority logic gate for magnetic quantum-dot cellular automata. *Science* [Online]. *311(5758)*, pp. 205–208. Available: http://www.sciencemag.org/cgi/content/abstract/311/5758/205

[10] M. C. B. Parish and M. Forshaw. (2003). Physical constraints on magnetic quantum cellular automata. *Appl. Phys. Lett.* [Online]. *83(10)*, pp. 2046–2048. Available: http://link.aip.org/link/?APL/83/2046/1

[11] G. Csaba and W. Porod, "Simulation of field coupled computing architectures based on magnetic dot arrays," *J. Comput. Electron.*, vol. 1, pp. 87–91, 2002.

[12] M. d'Aquino, "Nonlinear magnetization dynamics in thin-films and nanoparticles," Ph.D. dissertation, Università degli Study di Napoli "Federico II", Napoli, Italy, 2004

[13] A. Aharoni. (1998). Demagnetizing factors for rectangular ferromagnetic prisms. *J. Appl. Phys.* [Online]. *83(6)*, pp. 3432–3434. Available: http://link.aip.org/link/?JAP/83/3432/1

[14] B. Behin-Aein, S. Salahuddin, and S. Datta, "Switching energy of ferromagnetic logic bits," *IEEE Trans. Nanotechnol.*, vol. 8, no. 4, pp. 505–514, Jul. 2009.

[15] L. D. Landau and E. M. Lifshitz, "Theory of the dispersion of magnetic permeability in ferromagnetic bodies," *Phys. Z. Sowjetunion*, vol. 8, pp. 153–169, 1935.

[16] T. L. Gilbert, "A Lagrangian formulation of the gyromagnetic equation of the magnetic field," *Phys. Rev.*, vol. 100, p. 1243, 1955.

[17] C. E, J. Rantschler, S. Khizroev, and D. Litvinov. (2008). Micromagnetics of signal propagation in magnetic cellular logic data channels. *J. Appl. Phys.*[Online]. 104(5), pp. 054311-1–054311-4. Available: http://link.aip.org/link/?JAP/104/054311/1

[18] G. Csaba, A. Imre, G. Bernstein, W. Porod, and V. Metlushko, "Nanocomputing by field-coupled nanomagnets," *IEEE Trans. Nanotechnol.*, vol. 1, no. 4, pp. 209–213, Dec. 2002.

[19] J. Fidler and T. Schrefl, "Micromagnetic modelling : the current state of the art," *Appl. Phys. J. Phys. D*, vol. 33, no. 15, pp. R135–R156, 2000.

[20] J. Miltat, G. Albuquerque, and A. Thiaville, "An introduction to micromagnetics in the dynamic regime," in *Spin Dynamics in Confined Magnetic Structures*, vol. 83, Topics in Applied Physics, B. Hillebrands and K. Ounadjela, Eds., 2002, pp. 1–34.

[21] M. d'Aquino, C. Serpico, G. Coppola, I. D. Mayergoyz, and G. Bertotti. (2006). Midpoint numerical technique for stochastic landau-lifshitz-gilbert dynamics. *J. Appl. Phys.* [Online]. *99(8)*, pp. 08B905-1–08B905-3. Available: http://link.aip.org/link/?JAP/99/08B905/1

[22] D. B. Carlton, N. C. Emley, E. Tuchfeld, and J. Bokor. (2008). Simulation studies of nanomagnet-based logic architecture. *Nano Lett.* [Online]. *8(12)*, pp. 4173–4178. Available: http://pubs.acs.org/doi/abs/10.1021/nl801607p

[23] H. Bertram, V. Safonov, and Z. Jin, "Thermal magnetization noise, damping fundamentals, and mode analysis: application to a thin film gmr sensor," *IEEE Trans. Magn.*, vol. 38, no. 5, pp. 2514–2519, Sep. 2002.

[24] V. L. Safonov and H. N. Bertram. (2005). Fluctuation-dissipation considerations and damping models for ferromagnetic materials. *Phys. Rev. B (Condensed Matter Mater. Phys.)* [Online]. *71(22)*, pp. 224402-1–224402-5. Available: http://link.aps.org/abstract/PRB/v71/e224402

[25] S. Salahuddin and S. Datta. (2007). Interacting systems for self-correcting low power switching. *Appl. Phys. Lett.* [Online]. *90(9)*, pp. 093503-1–093503-3. Available: http://link.aip.org/link/?APL/90/093503/1

Federico M. Spedalieri received the M.Sc. degree in physics from the University of Buenos Aires, Buenos Aires, Argentina, in 1994, and the Ph.D. degree in physics from the California Institute of Technology, Pasadena, in 2003.

He is currently an Assistant Research Engineeer in the Department of Electrical Engineering, Univeristy of California, Los Angeles, where he is involved in research on fault tolerance, both in quantum and classical computing.

Ajey P. Jacob (M'07) received the B.Sc. degree in physics from the University of Kerala, Kerala, India, in 1994, the M.Sc. degree in applied physics from Maharaja Sayajirao University of Baroda, Vadodara, Gujarat, India, in 1996, and the Ph.D. degree in physics from the Department of Nanoelectronics and Microtechnology (MC2), Chalmers University of Technology/Gothenburg University, Sweden, in 2002.

In 2003, he cofounded the "Integrated Vertical Modules," a start-up firm to develop 3-D integration of silicon chips for memory applications using ion-cut technology. He joined Intel Corporation in 2004, Santa Clara, CA as a Device Engineer, where he supported its high-volume manufacturing and research activities in various capacities, and is currently a Research Scientist at the Technology Strategy Department, Technology and Manufacturing Group and technically managing the "Western Institute of Nanoelectronics"—industry government consortia, and other strategic research projects. From 2004 to 2006, he was the Intel Technical Lead for several sub-32-nm nanotechnology-related EU research projects. He was an Industry Mentor in both U.S. and European Universities for several Ph.D. students and Postdoctoral Fellows. He has authored or coauthored more than 50 articles in refereed journals and conferences.

Dmitri E. Nikonov (M'99–SM'06) received the M.S. degree in aeromechanical engineering from the Moscow Institute of Physics and Technology, Moscow, Zhukovsky, Russia, in 1992, and the Ph.D. degree in physics from Texas A&M University, College Station, in 1996.

He participated in the demonstration of world's first laser without population inversion at Texas A&M University. From 1997 to 1998, he was a Research Engineer and Lecturer at the Department of Electrical and Computer Engineering, University of California, Santa Barbara. in 1998, he joined Intel Corporation, Santa Clara, CA, where he is currently a Project Manager in the Components Research Division and is responsible for managing joint research programs with universities on nanoelectronics, spintronics, and material simulation. He was an Adjunct Associate Professor of electrical and computer engineering at Purdue University, Washington, DC during 2006. He has authored or coauthored 47 publications in refereed journals in quantum optics, free-electron, gas and semiconductor lasers, nanoelectronics, spintronics, and quantum device simulation, and holds 33 issued patents in optoelectronics, and integrated optic and spintronic devices.

Dr. Nikonov was a finalist for Best Doctoral Thesis competition of American Physical Society in 1997.

Vwani P. Roychowdhury received the Ph.D. degree in electrical engineering from Stanford University, Stanford, CA, in 1989.

From 1991 to 1996, he was a Faculty Member with the School of Electrical and Computer Engineering, Purdue University, West Lafayette, IN, where he became an Associate Professor in 1995. In 1996, he joined the University of California, Los Angeles, where he is currently a Professor of electrical engineering. He is also involved with the faculty of the Biomedical Engineering Interdepartamental Program. His research interests include models of computation, quantum and nanoelectronic computation, quantum information processing, fault-tolerant computation, combinatorics and information theory, advanced statistical processing, and adaptive algorithms.